WEP Warwick Evans Publishing

Transactions on Materials, Biotechnology and Life Sciences
ISSN: 2960-1932, eISSN: 2960-2319 | Volume 4
NSCBM 2024

Pharmacokinetics and Pharmacological/Bioactive Studies of Oridonin Derivatives in Anti-tumor Research

Yao Sang[1, *]

School of Life Sciences, Jilin University, Changchun City 130012, China

*Corresponding author: Yao Sang, e-mail: 13309173169@163.com

Abstract. Objective: it to investigate the pharmacokinetics of oridonin derivatives and their effects on tumor cell proliferation (Pro), invasion (Inv), and apoptosis (Apo), aiming to provide a theoretical basis for cancer treatment. Materials and Methods: drug and statistics (DAS) software was utilized to analyze the average blood concentration-time data collected, determining pharmacokinetic parameters. Human breast cancer MCF-7 cells were used as experimental cells. Cells were rolled into three groups: Group A (GA, 0 μM), Group B (GB, 2 μM), and Group C (GC, 4 μM) treated with 15 μL of different concentrations of oridonin derivative CYD0618. Cell Pro and cytotoxicity were evaluated using the MTT assay, while Apo, Inv, migration (Mig), and protein expression changes were assessed using flow cytometry, Transwell assays, and Western blotting, respectively. Results: over time, the average blood drug concentration gradually declined, notably within 5 hours. Pharmacokinetic analysis revealed initial distribution half-life (t1/2α) of approximately 2.104 hours, elimination half-life (t1/2β) of 69.303 hours, area under the concentration-time curve (AUC) of 41.637 mg/h/L, clearance rate (CL) of 0.089 L/h/kg, and apparent volume of distribution (V) of 0.4 L/kg. GB and GC exhibited greatly lower cell counts than GA ($P<0.05$), with GC showing fewer cells relative to GB ($P<0.05$). The Mig of tumor cells was notably reduced in GB and GC versus GA ($P<0.05$), and GC showed fewer migrated cells than GB ($P<0.05$). Furthermore, Inv of tumor cells was markedly lower in GB and GC versus GA ($P<0.05$), with GC demonstrating fewer invasive cells than GB ($P<0.05$). Apo rates were greatly higher in GB and GC relative to GA ($P<0.05$), and GC had a higher Apo rate than GB ($P<0.05$). Additionally, STAT3 and p-STAT3 levels were substantially higher in GB and GC versus GA ($P<0.05$), with GB showing notably higher p-STAT3 expression than GC ($P<0.05$). Conclusion: oridonin derivatives can inhibit tumor cell Pro, Inv, and Mig by suppressing STAT3 phosphorylation and promoting tumor cell Apo.

Keywords: oridonin derivatives; pharmacokinetics; anti-tumor; proliferation; migration and invasion; apoptosis.

1. Introduction

With the continuous increase in global cancer incidence, there is an urgent need in the medical research field to explore novel anti-cancer drugs that are highly efficient and low in toxicity. Natural products have long been recognized as significant sources for anti-cancer drug development due to their structural diversity, wide range of biological activities, and relatively low adverse effects [1,2]. Among these, oridonin, an active component extracted from the medicinal herb Rabdosia rubescens, has garnered considerable attention for its pronounced anti-inflammatory, antioxidant, and anti-tumor activities [3]. Oridonin, a flavonoid compound with multiple phenolic hydroxyl groups, has been shown to exert anti-cancer effects by modulating various signaling pathways, inhibiting tumor cell proliferation (*Pro*), inducing apoptosis (*Apo*), suppressing angiogenesis, and inhibiting metastasis [4,5]. Despite demonstrating promising anti-tumor activity, purified oridonin exhibits poor stability *in vivo* and struggles to achieve therapeutic blood concentrations, thereby limiting its clinical potential [6]. Therefore, the design and synthesis of oridonin derivatives aim to improve solubility, stability, and pharmacokinetic properties, thereby enhancing their *in vivo* anti-tumor efficacy.

Oridonin and its derivatives effectively inhibit the *Pro* of various cancer cells such as liver cancer, colon cancer, and leukemia by disrupting multiple molecular signaling pathways. They induce cell cycle arrest, block cell cycle progression, and activate caspase-dependent apoptotic pathways, leading

to programmed cell death in tumor cells [7]. Studies noted that oridonin derivatives also exert anti-tumor effects by modulating autophagy pathways [8]. Autophagy is a crucial cellular self-regulation mechanism involved in recycling cellular components and quality control. Certain derivatives can induce autophagic cell death in tumor cells, potentially through upregulating expression of autophagy-related genes and proteins (such as LC3-II) or inhibiting the activity of the autophagy suppressor mTOR [9]. In addition to directly impacting tumor cells, oridonin derivatives also inhibit the expression and activity of vascular endothelial growth factor and its receptors, thereby impeding formation of tumor neovasculature and cutting off the tumor's nutrient supply [10]. Furthermore, they downregulate proteins associated with tumor invasion (*Inv*) and metastasis, such as matrix metalloproteinases (MMPs), thereby inhibiting tumor spread and distant metastasis [11]. A deeper understanding of the anti-tumor mechanisms of oridonin derivatives helps clarify their targets, providing a theoretical basis for precision medicine. Modern techniques such as high-throughput screening and proteomic analysis can elucidate how these derivatives precisely regulate tumor-related signaling pathways and synergize with other therapeutic approaches [12].

This study analyzed the pharmacological and biological activities of oridonin derivatives, representing a crucial step towards their translation from laboratory research to clinical applications. Through interdisciplinary collaboration integrating knowledge and techniques from pharmacy, biology, and medicine, continual optimization of derivative structures was pursued. This approach aimed to deeply elucidate their mechanisms of action and develop more effective and safer anti-cancer drugs. These efforts held promise in providing new therapeutic avenues for cancer patients.

2. Materials and methodologies

2.1 Materials

The experimental materials included human breast cancer MCF-7 cells (Shanghai Zhaocai Biotechnology Co., Ltd., China); oridonin derivative CYD0618 (Wuhan Huajiu Pharmaceutical Technology Co., Ltd., China); male SD rats (Jinan Pengyue Experimental Animal Breeding Co., Ltd., China); oridonin reference standard (Shanghai Maclin Biochemical Technology Co., Ltd., China); cell *Pro* and cytotoxicity assay kits (MTT) (Shanghai Enzyme-linked Biotechnology Co., Ltd., China); acetonitrile, crystal violet staining solution (Beyotime Biotechnology Co., Ltd., China); HSTAT3, p-STAT3, and β-actin antibodies (Beijing Annoron Biological Technology Co., Ltd., China); phosphate-buffered saline (PBS) (Jingxin Biological Technology Co., Ltd., China); Annexin V-FITC solution and propidium iodide (Shanghai Weihuan Biological Technology Co., Ltd., China); trypsin-EDTA digestion solution, Dulbecco's Modified Eagle Medium (DMEM), and dimethyl sulfoxide (DMSO) (Shanghai Maclin Biochemical Technology Co., Ltd., China). The ethics committee of *** Hospital approved this work.

2.2 Pharmacokinetic experiments

The standard curve was established by precisely weighing 5.11 mg of oridonin reference standard, which was dissolved in methanol (10 mL) to prepare a stock solution of 511 μg/mL. This stock solution was further diluted to obtain a series of standard solutions of 0.303, 6.06, 12.12, 24.24, and 30.3 μg/mL. In addition, for the construction of the blood drug concentration-time curve, five sets of blank plasma (50 μL each) were prepared. To each set, 100 μL of the aforementioned different concentrations of oridonin reference standard solutions were added, resulting in plasma samples containing the drug reference solutions.

Five SD rats, weighing (230 ± 20) g, were selected for the study. They underwent a 12-hour fasting period with free access to water pre-experiment. During the trial, a suspension of oridonin derivative CYD0618 was prepared by intravenous injection via tail vein, with a dosage of 4 mg/kg in 0.5 mL. Subsequently, blood samples of 0.2 mL each were collected via retro-orbital bleeding at 0.5, 1, 2, 3, 4, 5, 6, 12, and 24 hours post-administration. Blood was collected using heparinized centrifuge tubes and centrifuged at 2,800 g for 10mins to obtain plasma. From each plasma sample, 100 μL was put

into 1.5 mL centrifuge tubes and mixed with 300 μL of acetonitrile by vortexing for 3mins. Supernatant was then harvested by centrifugation at 10,020 g for 10mins (Jining Jiuji Mechanical Equipment Co., Ltd., China) and used for analysis by high-performance liquid chromatography (HPLC) (Hangzhou Puyu Technology Development Co., Ltd., China).

Chromatographic analysis was implemented employing a Hypersil C18 analytical column (250mm×4.6mm, 5μm particle size) coupled with a pre-column (4mm×4mm, 5μm particle size). Mobile phase included methanol and water (60:40, v/v). Detection wavelength was 238 nm with a flow rate of 1 mL/min. Column temperature was 30°C, and injection volume was 20 μL. Chromatographic profiles of drug-free and drug-containing plasma were analyzed.

Pharmacokinetic parameters were analyzed using drug and statistics (DAS) software to analyze the collected average blood drug concentration-time data. Parameters determined included the initial distribution half-life (t1/2α), elimination half-life (t1/2β), area under the concentration-time curve (AUC), clearance rate (CL), and apparent volume of distribution (V) of the drug *in vivo*.

2.3 Cell grouping

MCF-7 cells were used as the experimental cells and were rolled into three groups: Group A (GA) received 0 μM concentration of oridonin derivative CYD0618, Group B (GB) received 2 μM, and Group C (GC) received 4 μM. Each group was treated with 15 μL of the respective concentration of CYD0618.

2.4 MTT assay for detecting cell *Pro*

MCF-7 cells were seeded into a 96-well culture plate, initially washed twice with PBS, followed by removal of the wash solution. Subsequently, cells were gently digested with 0.25% trypsin solution (0.5 mL) until round cell morphology was observed, after which the trypsin solution was aspirated. Cells were then supplemented with DMEM +10% fetal bovine serum (FBS), amino acids, and glucose, and dispersed into a uniform suspension by gentle pipetting, followed by cell counting. To achieve a target cell density of 4×10^5 cells/mL, the cell suspension was adjusted using DMEM supplemented with 10% FBS, and 100 μL adjusted cell suspension was applied to each well, ensuring three replicate wells per experimental condition for improved data reliability. Daily at specified time points, 5 mg/mL MTT solution (10 μL) was applied and cultured with cells in a 37°C, 5% CO_2 incubator for 4 hours to assess cell viability. After incubation, MTT was removed, and DMSO (150 μL) was applied to each well as a stop solution. The plates were gently shaken at 25°C for 10mins to dissolve the formazan crystals formed. Eventually, absorbance was measured at 490 nm employing an ELISA reader to quantify the cell survival or *Pro* capability.

2.5 Transwell assay for detecting cell migration (*Mig*)

During passaging, 100 μL of cell suspension was applied to Transwell inserts and cultured conventionally for 6 hours. Cell counting was performed using a hemocytometer, adjusting cell density to 4×10^5 cells/mL using DMEM +10% FBS. Matrigel-coated chambers were utilized to assess cell *Mig* capability. Subsequently, cells were rinsed with PBS and fixed with 95% ethanol for 10mins. Following air-drying, cells were stained with 4 g/L crystal violet solution for 20mins, followed by gentle wiping of non-migratory cells from the upper surface using a sterile cotton swab. After rinsing with PBS, cells were visualized under an E100 optical microscope (Nikon, Japan) and photographed for counting.

2.6 Transwell assay for detecting cell *Inv*

To begin, cell suspension (100 μL) was applied to the Transwell chamber and incubated under standard conditions for 6 hours. Cell counting was subsequently conducted using a hemocytometer, adjusting the cell density to 4×10^5 cells/mL with DMEM +10% FBS. Transwell upper chamber inserts, pre-coated with Matrigel gel, was filled with serum-free DMEM to assess cell *Inv* capability. Following incubation, cells were rinsed with PBS and fixed with 95% ethanol for 10mins, then stained

with a 4 g/L crystal violet solution for 20mins. After rinsing with PBS, cells were observed under an E100 optical microscope (Nikon, Japan) and photographed for counting purposes.

2.7 Detection of cell *Apo* by flow cytometry

After digestion of MCF-7 cells with trypsin, centrifugation was performed at 1,500 rpm for 3mins to remove supernatant. Subsequently, cell pellet was resuspended in appropriate culture medium to prepare a uniform cell suspension. Next, Annexin V-FITC solution (5 μL) was applied to each aliquot of cell suspension and thoroughly mixed, supplemented with propidium iodide (PI, 5 μL) and further mixing to ensure complete binding of the labeling molecules to the cells, then incubated at 25°C for 15mins to complete the labeling process for *Apo* and membrane permeability. Then, binding buffer (400 μL) was applied to each sample tube, and immediate preparation for flow cytometry analysis was conducted. The Attune CytPix flow cytometer from Thermo Fisher Scientific (USA), configured for precise detection of cell *Apo* and necrosis states, was utilized. This advanced instrument's analytical capabilities enabled efficient differentiation and quantification of cell populations in different states. Data were analyzed employing *FlowJo 7.6.1* from Becton, Dickinson and Company (BD, USA) to accurately calculate the proportion of cells undergoing *Apo*.

2.8 Western blot for detecting protein levels

MCF-7 cells were lysed in RIPA buffer for total protein extraction. BCA assay determined extracted total protein's concentration. Subsequently, proteins were separated on SDS-polyacrylamide gels for target protein separation, then transferred onto PVDF membranes, and blocked with 5% non-fat milk in TBST at 25°C for 2 hours. Membranes were then incubated overnight at 4°C with primary antibodies against STAT3, p-STAT3, and β-actin, then washed and incubated with HRP-conjugated secondary antibodies (diluted 1:5000 in TBST) at 25°C for 2 hours. ECL substrate visualized these protein bands, and images were captured using the Bio5000Plus gel imaging system (Bio-Rad, USA). *ImageJ* (National Institutes of Health, USA) was utilized for relative quantification of target protein expression levels.

2.9 Statistical methodologies

Data analysis and processing were conducted using *SPSS 19.0* (IBM, USA). Data were presented as mean ± standard deviation. One-way analysis of variance assessed differences among groups. Post hoc comparisons using the LSD test were conducted for data that met the assumption of homogeneity of variance. $P<0.05$ indicated statistical significance.

3. Results

3.1 Pharmacokinetic analysis of oridonin derivatives

Figure 1 shows the average blood concentration-time profile of oridonin derivative following intravenous tail vein injection in rats. It was evident that the average blood concentration decreased gradually over time, with a more pronounced decrease within the first five hours. Data analysis using DAS software revealed the following key pharmacokinetic parameters: the t1/2α of the drug in the body was approximately 2.104 hours, the t1/2β was 69.303 hours, the AUC was 41.637 mg/h/L, the CL was 0.089 L/h/kg, and the V was 0.4 L/kg.

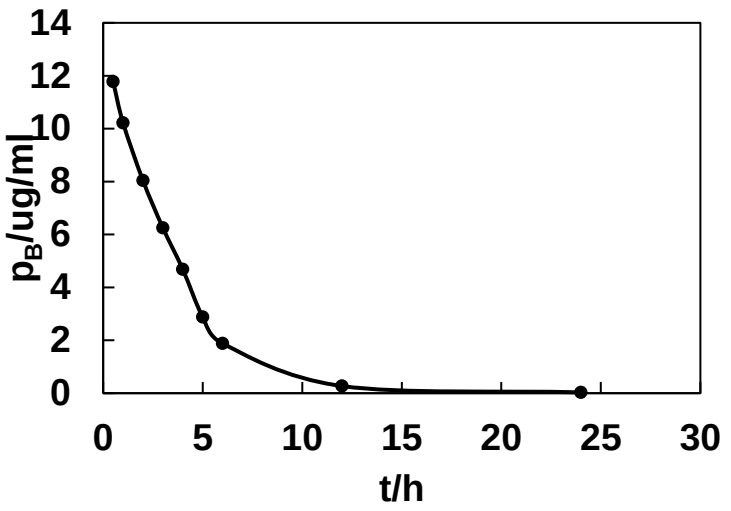

Figure. 1 Average blood concentration-time curve after intravenous injection of oridonin derivatives in rats.

3.2 Effects of oridonin derivatives on *Pro* of tumor cells

Figure 2 depicts the impact of oridonin derivatives on tumor cell *Pro*. It was evident that cell counts in GB and GC were substantially inferior to in GA (P<0.05), and cell counts in GC were markedly inferior to in GB (P<0.05).

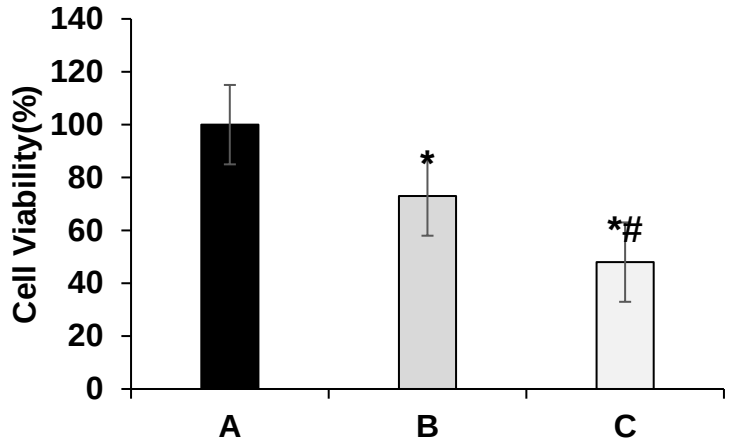

Figure. 2 Impacts of oridonin derivatives on Pro of tumor cells. (* indicated P<0.05 vs. GA, # indicated P<0.05 vs. GB (in all figures below).)

3.3 Effects of oridonin derivatives on *Mig* of tumor cells

Figure 3 illustrates the influence of oridonin derivatives on tumor cell *Mig*. It was evident that the GB and GC demonstrated notably inferior number of migrated tumor cells to GA (P<0.05), and that in GC was considerably inferior to GB (P<0.05).

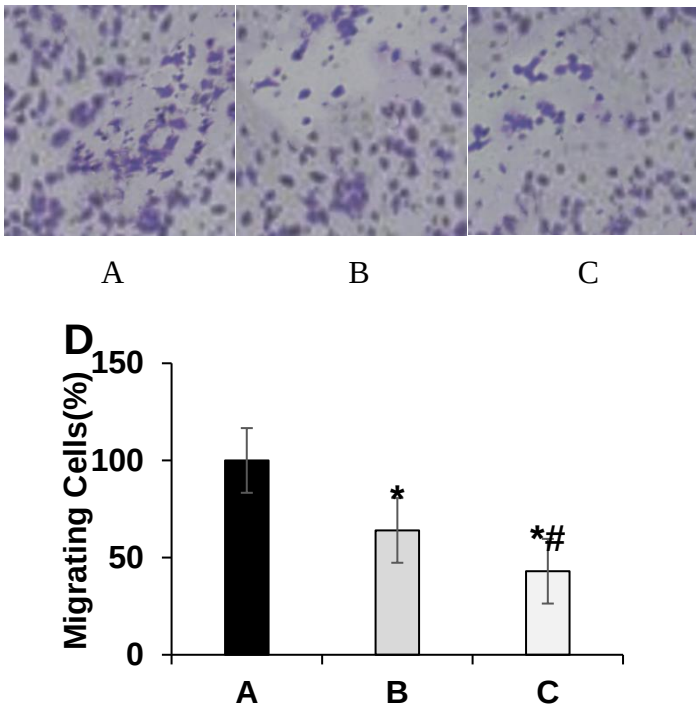

Figure. 3 Influences of oridonin derivatives on Mig of tumor cells. (A, B, C represent Transwell Mig staining results of GA, GB, and GC cells, respectively; D shows the number of migrated cells.)

3.4 Effects of oridonin derivatives on *Inv* of tumor cells

Figure 4 presents the influence of oridonin derivatives on tumor cell *Inv*. The data indicated that GB and GC exhibited greatly fewer invading tumor cells relative to GA ($P<0.05$). Additionally, GC showed a notable reduction in invading tumor cells versus GB ($P<0.05$).

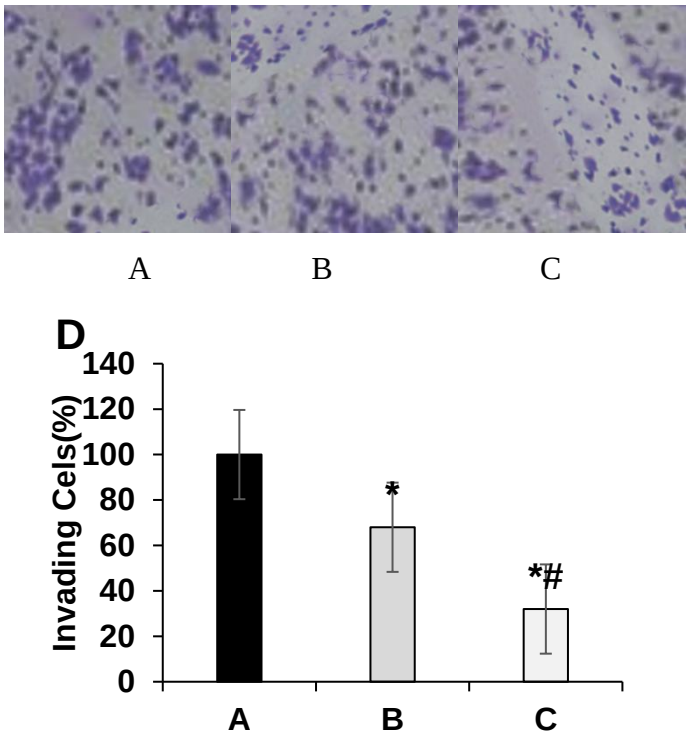

Figure. 4 Effects of oridonin derivatives on Inv of tumor cells. (A, B, C represent Transwell Inv staining results of GA, GB, and GC cells, respectively; D shows the number of invading cells.)

3.5 Effects of oridonin derivatives on *Apo* of tumor cells

Figure 5 depicts the impact of oridonin derivatives on *Apo* in tumor cells. The results indicated that GB and GC exhibited markedly higher *Apo* rates relative to GA ($P<0.05$). Moreover, GC showed a markedly higher *Apo* rate than GB ($P<0.05$).

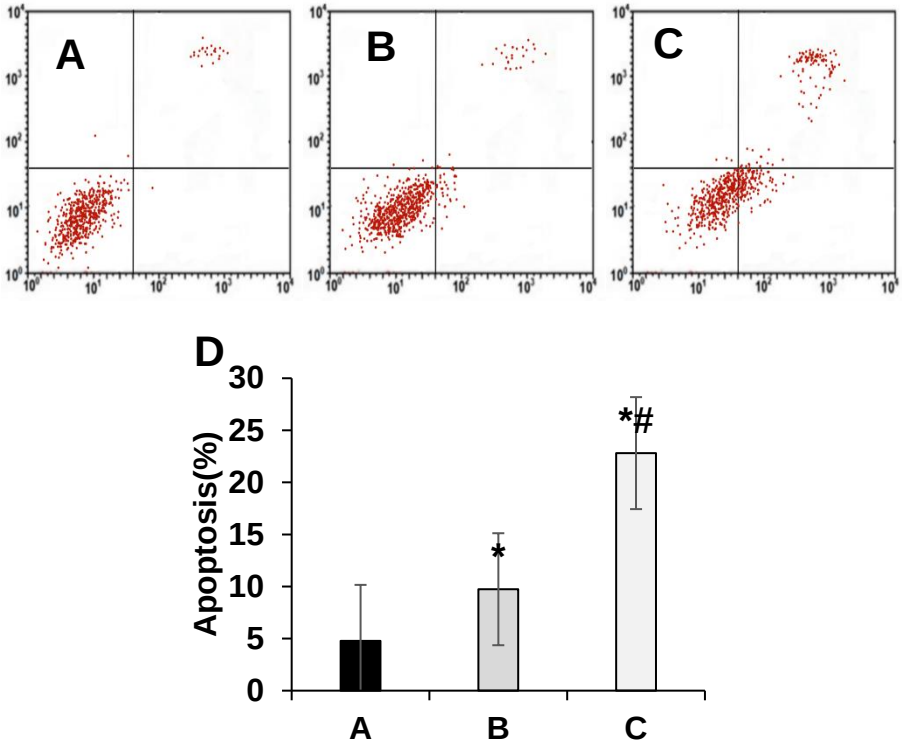

Figure. 5 Effects of oridonin derivatives on Apo in tumor cells. (A, B, C represent flow cytometry plots of GA, GB, and GC cells, respectively; D shows apoptotic rate.)

3.6 Effects of oridonin derivatives on STAT3 protein level and phosphorylation in tumor cells

Figure 6 illustrates the effects of oridonin derivatives on STAT3 protein level and phosphorylation in tumor cells. It was revealed that GB and GC exhibited notably higher levels of STAT3 and p-STAT3 expression versus GA ($P<0.05$). Additionally, GB showed greatly higher p-STAT3 expression relative to GC ($P<0.05$).

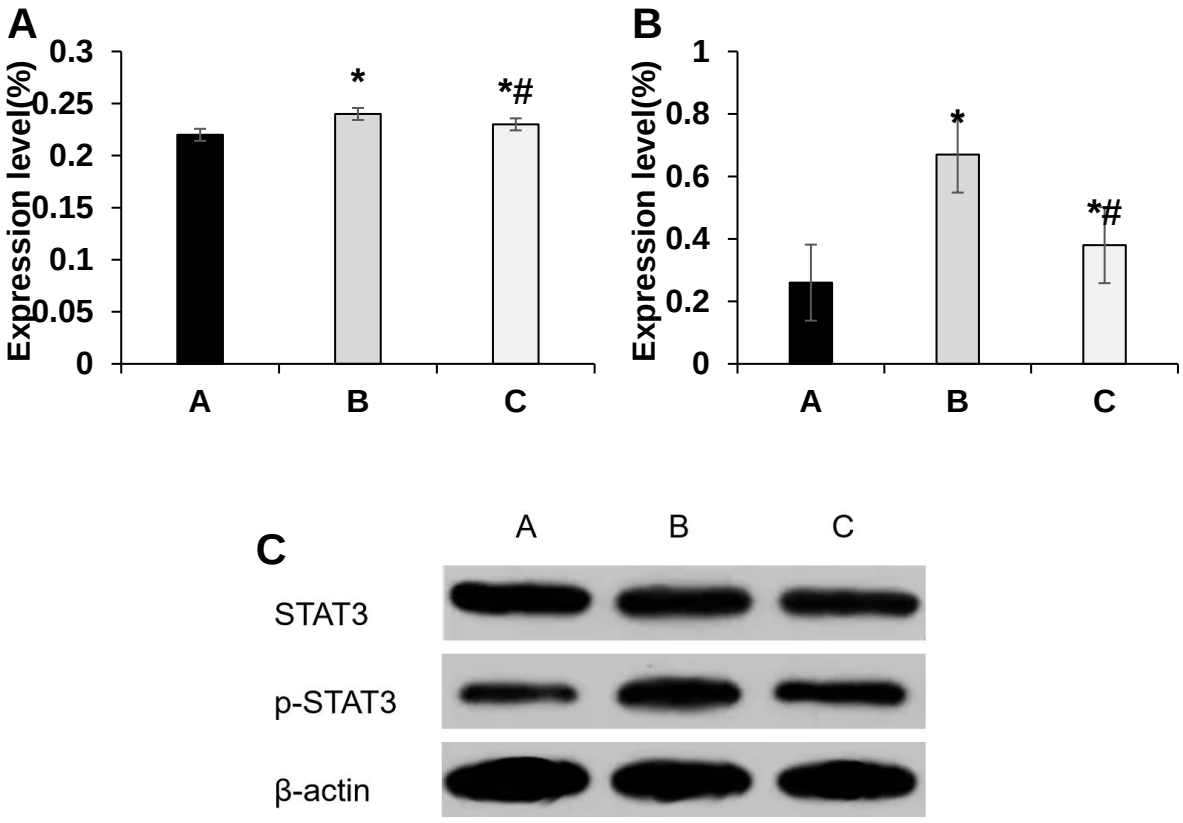

Figure. 6 Effects of oridonin derivatives on STAT3 protein expression and phosphorylation in tumor cells. (A represents STAT3, B represents p-STAT3, C represents Western blot images.)

4. Discussion

Oridonin, as a natural product, exhibits broad-spectrum anti-tumor activity by targeting multiple mechanisms in cancer cells, offering new possibilities for cancer treatment. This study investigated the pharmacokinetics of oridonin and the effects of oridonin derivatives on *Pro*, *Mig*, *Inv*, and *Apo* of human breast cancer MCF-7 cells. The study also analyzed the impact of oridonin derivatives on STAT3 protein level and phosphorylation in MCF-7 cells. The findings demonstrated that oridonin derivative CYD0618 inhibited *Pro*, *Mig*, and *Inv* while promoting *Apo* in MCF-7 cells. Moreover, it suppresses STAT3 protein phosphorylation in MCF-7 cells, indicating promising anti-tumor effects against human breast cancer.

In this study, DAS software was employed to analyze the collected data on the average blood concentration-time profile of oridonin PLGA nanoparticles in rats. The aim was to characterize the pharmacokinetic properties using a two-compartment model, which best described the dynamic distribution and elimination processes of the drug in the rat body. By comparing the goodness of fit among different models, the two-compartment model was found to best fit the study data, effectively illustrating the drug's distribution and elimination kinetics. According to the analysis using the two-compartment model, key pharmacokinetic parameters were determined: the t1/2α of the drug in the body was approximately 2.104 hours, reflecting its rapid distribution to various tissues. The t1/2β was extended, lasting 69.303 hours, indicating a relatively slow elimination process from the body. The AUC was calculated as 41.637 mg·h/L, representing the total exposure of the drug in the body. Additionally, the CL was 0.089 L/h/kg, revealing the rate at which the drug was cleared from the body per unit of time. V was 0.4 L/kg, suggesting the theoretical volume occupied by the drug when uniformly distributed in the body. These parameters collectively delineate the absorption, distribution, metabolism, and excretion characteristics of oridonin PLGA nanoparticles in rats.

The results demonstrated that the oridonin derivative CYD0618 effectively inhibited *Pro*, *Mig*, and *Inv* of human breast cancer MCF-7 cells, with stronger inhibitory effects observed at higher concentrations. CYD0618 also promoted *Apo* in these cells, with a more pronounced effect at higher concentrations. Compared to the parent compound oridonin, CYD0618 has undergone specific structural modifications that enhance its interaction with specific targets within breast cancer cells. This modification enables CYD0618 to penetrate cell membranes more effectively, bind to proteins more stably, or bind more selectively to key signaling molecules, thereby enhancing its biological activity [13,14]. CYD0618 disrupts the cell cycle progression of breast cancer cells, leading to cell cycle arrest [15]. Furthermore, it may inhibit the expression of molecules associated with cell *Mig* and *Inv*, such as matrix metalloproteinases (MMPs) and cell adhesion molecules, thereby reducing extracellular matrix degradation and disruption of intercellular connections, thereby inhibiting tumor *Inv* and metastasis [16,17]. CYD0618 potentially induces cell *Apo* through activation of endogenous pathways, such as the mitochondrial pathway, leading to cytochrome C release, activation of caspase cascades, and DNA fragmentation, ultimately resulting in cell *Apo* [18,19]. It may also promote *Apo* by modulating Bcl-2 family proteins or inhibiting anti-apoptotic signaling pathways. Studies by Kazantseva et al. (2022) [20] suggested that CYD6-17 exhibits inhibitory effects on bladder cancer, with these derivatives typically enhancing intervention in specific signaling pathways or improving pharmacokinetic properties to achieve stronger anti-tumor effects. Research by Hua et al. (2021) [21] indicated that natural product derivatives like CYD0618 often exhibit lower systemic toxicity and better selectivity compared to traditional chemotherapy drugs. They are capable of targeting more specifically the biological characteristics of tumor cells, thereby reducing damage to normal cells.

This study demonstrated that high concentrations of the oridonin derivative CYD0618 inhibited STAT3 protein phosphorylation in MCF-7 cells. Aberrant activation of STAT3, particularly sustained phosphorylation, is common in various types of cancer and is associated with tumor initiation, progression, *Inv*, and metastasis [22,23]. Research indicated that oridonin significantly inhibits STAT3 phosphorylation; Western blotting and similar techniques have shown decreased phosphorylated STAT3 (p-STAT3) in tumor cells treated with oridonin. This suggests that oridonin disrupts the IL-6/STAT3 signaling pathway [24], which is typically activated in inflammation and the tumor microenvironment, promoting tumor cell *Pro* and survival [25]. Oridonin reduces the level of p-STAT3, thereby decreasing the expression of downstream pro-proliferative genes and inhibiting tumor cell *Pro* [26]. Simultaneously, oridonin inhibits STAT3 phosphorylation to restore the activity of *Apo*-related proteins and reduce the expression of anti-apoptotic proteins, promoting tumor cell *Apo* [27]. Oridonin-mediated dephosphorylation of STAT3 may also regulate autophagy-related genes such as LC3 and Beclin-1, thereby enhancing autophagic cell death in tumor cells [28]. By inhibiting STAT3 phosphorylation, oridonin not only directly affects tumor cell *Pro* and survival mechanisms but also potentially improves the tumor microenvironment, offering a novel perspective for anti-cancer therapy [29,30].

5. Conclusion

This study investigated the pharmacokinetics of oridonin and the effects of its derivative CYD0618 on *Pro*, *Apo*, *Mig*, and *Inv* of MCF-7 cells. It was revealed that CYD0618 promoted STAT3 protein phosphorylation, thereby regulating multiple aspects of *Pro*, *Apo*, *Mig*, and *Inv* in MCF-7 cells. These mechanisms underscore the remarkable promotive role of CYD0618 in breast cancer. Limitations of this study include its exclusive focus on cell experiments without validation in clinical samples, as well as the lack of exploration into the effects of other oridonin derivatives. Future research should validate these findings in clinical samples and investigate the anti-tumor effects of other oridonin derivatives.

References

[1] Zhou F, Gao H, Shang L, Li J, Zhang M, Wang S, Li R, Ye L, Yang S. Oridonin promotes endoplasmic reticulum stress via TP53-repressed TCF4 transactivation in colorectal cancer. J Exp Clin Cancer Res. 2023 Jun 19;42(1):150. doi: 10.1186/s13046-023-02702-4. PMID: 37337284; PMCID: PMC10278272.

[2] Hwang TL, Chang CH. Oridonin enhances cytotoxic activity of natural killer cells against lung cancer. Int Immunopharmacol. 2023 Sep; 122:110669. doi: 10.1016/j.intimp.2023.110669. Epub 2023 Jul 20. PMID: 37480753.

[3] Zhang W, Shi L, Zhou W, Liu X, Xi Y, Wang X, Li Y, Xu X, Tang Y. Oridonin impedes breast cancer growth by blocking cells in S phase and inhibiting the PI3K/AKT/mTOR signaling pathway. Heliyon. 2023 Jul 11;9(7): e18046. doi: 10.1016/j.heliyon.2023.e18046. PMID: 37519735; PMCID: PMC10372243.

[4] Gao S, Tan H, Li D. Oridonin suppresses gastric cancer SGC-7901 cell proliferation by targeting the TNF-alpha/androgen receptor/TGF-beta signalling pathway axis. J Cell Mol Med. 2023 Sep;27(18):2661-2674. doi: 10.1111/jcmm.17841. Epub 2023 Jul 11. PMID: 37431884; PMCID: PMC10494293.

[5] Gao J, Li C, Wang X, Sun X, Zhang R, Chen C, Yu M, Liu Y, Zhu Y, Chen J. Oridonin attenuates lung inflammation and fibrosis in silicosis via covalent targeting iNOS. Biomed Pharmacother. 2022 Sep; 153: 113532. doi: 10.1016/j.biopha.2022.113532. Epub 2022 Aug 10. PMID: 36076611.

[6] Liu W, Wang X, Wang L, Mei Y, Yun Y, Yao X, Chen Q, Zhou J, Kou B. Oridonin represses epithelial-mesenchymal transition and angiogenesis of thyroid cancer via downregulating JAK2/STAT3 signaling. Int J Med Sci. 2022 May 27;19(6):965-974. doi: 10.7150/ijms.70733. PMID: 35813296; PMCID: PMC9254367.

[7] Cai M, Yao Y, Yin D, Zhu R, Fu T, Kong J, Wang K, Liu J, Yao A, Ruan Y, Shi W, Zhu Q, Ni J, Yin X. Enhanced lysosomal escape of cell penetrating peptide-functionalized metal-organic frameworks for co-delivery of survivin siRNA and oridonin. J Colloid Interface Sci. 2023 Sep 15; 646: 370-380. doi: 10.1016/j.jcis.2023.04.126. Epub 2023 Apr 28. PMID: 37207419.

[8] Wang Y, Wang M, Lin F, Zhang X, Zhao Y, Guo C, Wang J. Preparation, Characterization, and Evaluation of Liposomes Containing Oridonin from Rabdosia rubescens. Molecules. 2022 Jan 27;27(3):860. doi: 10.3390/molecules27030860. PMID: 35164121; PMCID: PMC8839758.

[9] Chen L, Li D, Guo X, Cheng C, Wei X. Oridonin Synergistically Enhances the Pro-Apoptotic Effect of Venetoclax on Acute Myeloid Leukemia Cells by Inhibiting AKT Signaling. Front Biosci (Landmark Ed). 2023 Sep 6;28(9):195. doi: 10.31083/j.fbl2809195. PMID: 37796705.

[10] Xu L, Jiang Y, Bi Y, Zheng S, Wu Y, Wu Y, Xu Y, Chen J. Suppression of PERK/eIF2α/CHOP pathway enhances oridonin-induced apoptosis by inhibiting autophagy in Small-Cell lung cancer cells. Biomed Pharmacother. 2024 Jun; 175: 116684. doi: 10.1016/j.biopha.2024.116684. Epub 2024 May 6. PMID: 38713951.

[11] Jin X, Xu J, Yang F, Chen J, Luo F, Xu B, Xu J. Oridonin Attenuates Thioacetamide-Induced Osteoclastogenesis Through MAPK/NF-κB Pathway and Thioacetamide-Inhibited Osteoblastogenesis Through BMP-2/RUNX2 Pathway. Calcif Tissue Int. 2023 Jun;112(6):704-715. doi: 10.1007/s00223-023-01080-5. Epub 2023 Apr 9. PMID: 37032340; PMCID: PMC10198936.

[12] Chen B, Liu X, Li Y, Shan T, Bai L, Li C, Wang Y. iRGD Tumor-Penetrating Peptide-Modified Nano-Delivery System Based on a Marine Sulfated Polysaccharide for Enhanced Anti-Tumor Efficiency Against Breast Cancer. Int J Nanomedicine. 2022 Feb 9; 17: 617-633. doi: 10.2147/IJN.S343902. PMID: 35173433; PMCID: PMC8842734.

[13] Yang H, Wang J, Khan S, Zhang Y, Zhu K, Zhou E, Gong M, Liu B, Kan Q, Zhang Q. Selective synergistic anticancer effects of cisplatin and oridonin against human p53-mutant esophageal squamous carcinoma cells. Anticancer Drugs. 2022 Jan 1;33(1): e444-e452. doi: 10.1097/CAD.0000000000001237. PMID: 34520434; PMCID: PMC8670348.

[14] Zhang S, Vijayalakshmi A, Meng L. Oridonin attenuated human PC-3 cell activity by modulating the Wnt/β-catenin signaling. Adv Clin Exp Med. 2024 May;33(5):511-518. doi: 10.17219/acem/175519. PMID: 38269477.

[15] Wu G, Guo Y, Liu Y, Cai X, Deng T, Pei T, Huang L, Chen K, Pan X. Network-Based Method to Investigate the Promoted Cell Apoptosis Mechanisms of Oridonin in OSCC through the RNA-Transcriptome. J Immunol Res. 2023 Mar 16; 2023: 5293677. doi: 10.1155/2023/5293677. PMID: 36969496; PMCID: PMC10036191.

[16] Sun H, Nai J, Deng B, Zheng Z, Chen X, Zhang C, Sheng H, Zhu L. Angelica Sinensis Polysaccharide-Based Nanoparticles for Liver-Targeted Delivery of Oridonin. Molecules. 2024 Feb 5; 29(3): 731. doi: 10.3390/molecules29030731. PMID: 38338476; PMCID: PMC10856552.

[17] Wu Q, Gao X, Lin Y, Wu C, Zhang J, Chen M, Wen J, Wu Y, Tian K, Bao W, Sun P, Zhu A. Integrating Epigenetics, Proteomics, and Metabolomics to Reveal the Involvement of Wnt/β-Catenin Signaling Pathway in Oridonin-Induced Reproductive Toxicity. Toxics. 2024 May 7;12(5):339. doi: 10.3390/toxics12050339. PMID: 38787118; PMCID: PMC11126149.

[18] Zhou J, Li Y, Shi X, Hao S, Zhang F, Guo Z, Gao Y, Guo H, Liu L. Oridonin inhibits tumor angiogenesis and induces vessel normalization in experimental colon cancer. J Cancer. 2021 Apr 2; 12(11): 3257-3264. doi: 10.7150/jca.55929. PMID: 33976735; PMCID: PMC8100792.

[19] Liu X, Xu J, Zhou J, Shen Q. Oridonin and its derivatives for cancer treatment and overcoming therapeutic resistance. Genes Dis. 2020 Jul 5;8(4):448-462. doi: 10.1016/j.gendis.2020.06.010. PMID: 34179309; PMCID: PMC8209342.

[20] Kazantseva L, Becerra J, Santos-Ruiz L. Oridonin enhances antitumor effects of doxorubicin in human osteosarcoma cells. Pharmacol Rep. 2022 Feb;74(1):248-256. doi: 10.1007/s43440-021-00324-1. Epub 2021 Aug 24. PMID: 34427908; PMCID: PMC8786785.

[21] Hua X, Wu P, Gao GS, Ye XL. Combination of oridonin and TRAIL induces apoptosis in uveal melanoma cells by upregulating DR5. Int J Ophthalmol. 2021 Dec 18;14(12):1834-1842. doi: 10.18240/ijo.2021.12.05. PMID: 34926196; PMCID: PMC8640766.

[22] Abdullah NA, Md Hashim NF, Ammar A, Muhamad Zakuan N. An Insight into the Anti-Angiogenic and Anti-Metastatic Effects of Oridonin: Current Knowledge and Future Potential. Molecules. 2021 Feb 3;26(4):775. doi: 10.3390/molecules26040775. PMID: 33546106; PMCID: PMC7913218.

[23] Liu W, Huang G, Yang Y, Gao R, Zhang S, Kou B. Oridonin inhibits epithelial-mesenchymal transition of human nasopharyngeal carcinoma cells by negatively regulating AKT/STAT3 signaling pathway. Int J Med Sci. 2021 Jan 1;18(1):81-87. doi: 10.7150/ijms.48552. PMID: 33390776; PMCID: PMC7738957.

[24] Che X, Zhan J, Zhao F, Zhong Z, Chen M, Han R, Wang Y. Oridonin Promotes Apoptosis and Restrains the Viability and Migration of Bladder Cancer by Impeding TRPM7 Expression via the ERK and AKT Signaling Pathways. Biomed Res Int. 2021 Jul 5;2021:4340950. doi: 10.1155/2021/4340950. PMID: 34285910; PMCID: PMC8275389.

[25] Tan RZ, Yan Y, Yu Y, Diao H, Zhong X, Lin X, Liao YY, Wang L. Renoprotective Effect of Oridonin in a Mouse Model of Acute Kidney Injury via Suppression of Macrophage Involved Inflammation. Biol Pharm Bull. 2021;44(5):714-723. doi: 10.1248/bpb.b21-00071. PMID: 33952827.

[26] He S, Tian S, He X, Le X, Ning Y, Chen J, Chen H, Mu J, Xu K, Xiang Q, Wu Y, Chen J, Xiang T. Multiple targeted self-emulsifying compound RGO reveals obvious anti-tumor potential in hepatocellular carcinoma. Mol Ther Oncolytics. 2021 Aug 19;22:604-616. doi: 10.1016/j.omto.2021.08.008. PMID: 34589579; PMCID: PMC8449031.

[27] Yan SL, Huang CS, Mong MC, Yin MC. Oridonin Attenuates the Effects of Chronic Alcohol Consumption Inducing Oxidative, Glycative and Inflammatory Injury in the Mouse Liver. In Vivo. 2021 Jul-Aug;35(4):2141-2149. doi: 10.21873/invivo.12484. PMID: 34182490; PMCID: PMC8286538.

[28] Fan X, Wang T, Ji Z, Li Q, Shen H, Wang J. Synergistic combination therapy of lung cancer using lipid-layered cisplatin and oridonin co-encapsulated nanoparticles. Biomed Pharmacother. 2021 Sep;141:111830. doi: 10.1016/j.biopha.2021.111830. Epub 2021 Jun 17. PMID: 34146851.

[29] Liu Y, Song Z, Liu Y, Ma X, Wang W, Ke Y, Xu Y, Yu D, Liu H. Identification of ferroptosis as a novel mechanism for antitumor activity of natural product derivative a2 in gastric cancer. Acta Pharm Sin B. 2021 Jun;11(6):1513-1525. doi: 10.1016/j.apsb.2021.05.006. Epub 2021 May 13. PMID: 34221865; PMCID: PMC8245858.

[30] Tan Y, Zhou X, Gong Y, Gou K, Luo Y, Jia D, Dai L, Zhao Y, Sun Q. Biophysical and biochemical properties of PHGDH revealed by studies on PHGDH inhibitors. Cell Mol Life Sci. 2021 Dec 31;79(1):27. doi: 10.1007/s00018-021-04022-2. PMID: 34971423; PMCID: PMC11073335.